Broadband and chiral binary dielectric meta-holograms

The Harvard community has made this article openly available. Please share how this access benefits you. Your story matters

APPLIED OPTICS

Broadband and chiral binary dielectric meta-holograms

Mohammadreza Khorasaninejad,[1]* Antonio Ambrosio,[1,2]* Pritpal Kanhaiya,[1,3] Federico Capasso[1†]

Subwavelength structured surfaces, known as meta-surfaces, hold promise for future compact and optically thin devices with versatile functionalities. By revisiting the concept of detour phase, we demonstrate high-efficiency holograms with broadband and chiral imaging functionalities. In our devices, the apertures of binary holograms are replaced by subwavelength structured microgratings. We achieve broadband operation from the visible to the near infrared and efficiency as high as 75% in the 1.0 to 1.4 μm range by compensating for the inherent dispersion of the detour phase with that of the subwavelength structure. In addition, we demonstrate chiral holograms that project different images depending on the handedness of the reference beam by incorporating a geometric phase. Our devices' compactness, lightness, and ability to produce images even at large angles have significant potential for important emerging applications such as wearable optics.

INTRODUCTION

Holography—the branch of optics that uses the whole (ὅλος in Greek) information (amplitude and phase) of light—represented a major step forward in optical science during the second half of the last century (1). Although an interference pattern had to be initially recorded in photographic plates, the principle of holography has since greatly expanded visualization possibilities (2, 3) and applications (4, 5), in particular through the widespread use of computer-generated holograms (6). Holographic principles have been applied to overcome experimental challenges where other approaches have failed. This has been the case, for instance, with imaging through diffusive media (7) and the realization of portable three-dimensional projectors (4, 8). Nowadays, the enormous progress in nanofabrication techniques may revolutionize holography just as the invention of the laser did many years ago. Subwavelength structured optical elements (gratings, etc.) (9) and, more generally, metamaterials (10) and meta-surfaces (11–30)—with their ability to control phase, amplitude, and polarization over subwavelength scales without requiring volumetric propagation—are opening new frontiers in holographic and optical devices such as wearable displays. However, to the best of our knowledge, in all of these implementations, the wavelength response is highly dispersive, and highly efficient operation has been limited to reflection-mode configurations.

Here, we show how basic holographic principles can be revisited to implement new capabilities of wavefront molding with planar subwavelength dielectric optical elements. Our holographic devices are transmissive, broadband, and phase distortion–free from the near-infrared (NIR) range to the visible range, with high polarization sensitivity allowing for a wide range of functionalities depending on the design. The basic element of our holograms (Fig. 1) is an "effective aperture" designed to diffract light with high efficiency across a broad range of wavelengths into the (±1) diffraction order; thus, it is functionally equivalent to a broadband blazed grating. The phase profile of our meta-holograms is then generated by displacing the effective apertures with respect to each other

in such a way as to create the desired interference pattern. The latter is the detour phase concept, which is the basis of binary holograms. A complex computer-generated hologram representing the logo of the International Year of Light (IYL) has been imaged with high efficiency (up to 75%) in the NIR range. By further incorporating a lens into the hologram, the effective focal length of the imaging system has been shifted by a controlled amount. Polarization-selective holograms have been widely investigated (20–22); here, we have demonstrated a chiral holographic plate that creates different images depending on the handedness of the incident light.

DESIGN OF DISPERSIONLESS META-HOLOGRAMS

Lord Rayleigh and, later, Michelson (31) observed how periodic errors in grating fabrication affect the interference pattern by modulating the wavefront. This concept of wavefront shaping through displacement of adjacent elements, known as detour phase, has been perfected and used in the first computer-generated holograms. Detour phase is the design principle of our devices (2, 32, 33) and is the core concept behind binary holograms, where the amplitude and the phase of the optical field are imposed by an array of apertures on an opaque screen. In a typical binary hologram, the dimension of each aperture sets the amount of light passing through it. The phase shift of the light diffracted from two adjacent apertures along a given direction (θ) (Fig. 1A) is controlled by adjusting the distance between them. The light wavelets from the two apertures are in-phase if the distance D between them is $n\lambda/\sin(\theta)$, where n is an integer and λ is the wavelength. For any other distance, the wavelets from the two apertures will be phase-shifted relative to each other by the amount

$$\Delta\varphi = \frac{2\pi D}{\lambda}\sin(\theta) \qquad (1)$$

The wavelength dependence of this phase shift can be suppressed if diffraction from the apertures is designed in such a way as to compensate for the intrinsic dispersion. From Eq. 1, one can see that this dispersionless condition can be achieved if each aperture is replaced by a subwavelength

[1]Harvard John A. Paulson School of Engineering and Applied Sciences, Harvard University, Cambridge, MA 02138, USA. [2]CNR-SPIN Sede secondaria di Napoli, Dipartimento di Fisica, Università di Napoli Federico II, Complesso Universitario di Monte Sant'Angelo, Via Cintia, Napoli 80126, Italy. [3]University of Waterloo, Waterloo, Ontario N2L 3G1, Canada.
*These authors contributed equally to this work.
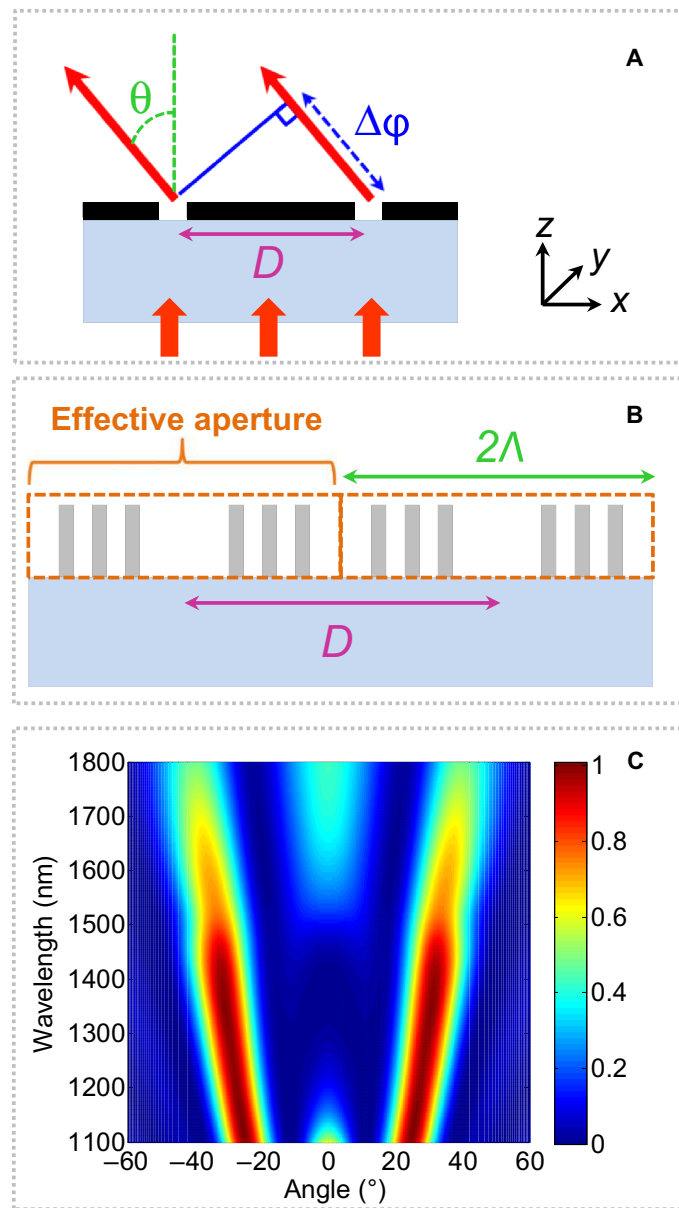†Corresponding author. Email: capasso@seas.harvard.edu

structured element (meta-element) with an engineered dispersion similar to that of gratings, that is, $\sin(\theta) \sim \lambda$.

Current lithography techniques allow surface structuring with subwavelength resolution. In our devices, the apertures are replaced by effective apertures (pixels) with a polarization functionality provided by the specifically incorporated meta-element. For the first study, the meta-element consists of three dielectric ridge waveguides (DRWs), made of amorphous silicon, on a glass substrate (fig. S1). A diffraction condition where most of the transmitted light is funneled into the first orders (±1) is achieved by adjusting the DRW design parameters (width, height, and separation) and the lateral dimension Λ of the meta-element (fig. S2). In our design, each pixel of dimension 2Λ consists of two of such meta-elements, that is, six amorphous silicon ridges (Fig. 1B). Figure 1C shows that the transmitted power from each pixel is nearly completely split between the +1 order and the −1 order in a broad wavelength range (1100 to 1800 nm), whereas unwanted orders are suppressed. The dispersive response of the pixel is designed with finite-difference time domain simulations to closely satisfy the relation $\theta = \sin^{-1}(\lambda/\Lambda)$ (Fig. 2A), to achieve a wavelength-independent phase shift $\Delta\varphi$, as previously discussed.

If we now design a hologram out of these effective apertures, the phase shift of the light diffracted by each aperture along the direction θ— defined relative to the light from a reference aperture propagating along the same direction θ—is still given by Eq. 1. Substituting $\theta = \sin^{-1}(\lambda/\Lambda)$ into Eq. 1 then yields the dispersionless detour phase

$$\Delta\varphi\,(x_m, y_m)\;=\;\frac{2\pi D\,(x_m, y_m)}{\Lambda} \tag{2}$$

where (x_m, y_m) are the coordinates of the pixels' centers and the index m spans over the total number of pixels.

Although the description of our pixels as effective apertures is useful, our devices have no opaque screen or apertures but a transparent glass substrate whose surface is structured in pixels displaced with respect to each other to obtain the required phase map. The desired phase distribution that will generate the intensity pattern of interest when illuminated by the reference beam is then computed by means of the widely used Gerchberg-Saxton phase-retrieval algorithm (34) (see the Supplementary Materials). The computed phase map is then converted into a spatial distribution of displacements $D(x_m, y_m)$ that defines the equivalent of a binary phase–only hologram. In our design, the light diffracted by two adjacent pixels is in-phase if the pixels' centers are spaced by 2Λ, that is, the two effective apertures are touching (Fig. 1B). The desired phase modulation is then achieved by displacing each pixel with respect to the in-phase condition. This design represents the highest possible pixel density. We chose this configuration to maximize the total cross section of the device to the illuminating light, minimizing the spacing between adjacent pixels and the light that passes through nondiffracted. This configuration results in the physical overlap of a certain amount of effective apertures. In the design process, we removed the DRWs that physically overlapped (less than 5% of the total number), whereas we kept all the six ridges when the pixel overlap only affected the area without DRWs. An example of this condition is highlighted in the inset to Fig. 2C. The pixels containing blue and red DRWs partially overlap by design. Such partial overlap only affects the amount of light along θ from those pixels and results in a possible decrease in the contrast of the image in the Fourier plane (random amplitude modulation). However, the high quality of the images obtained proves that this effect is negligible in our devices. Furthermore, this type of phase modulation allows 0 to 2π continuous phase variation
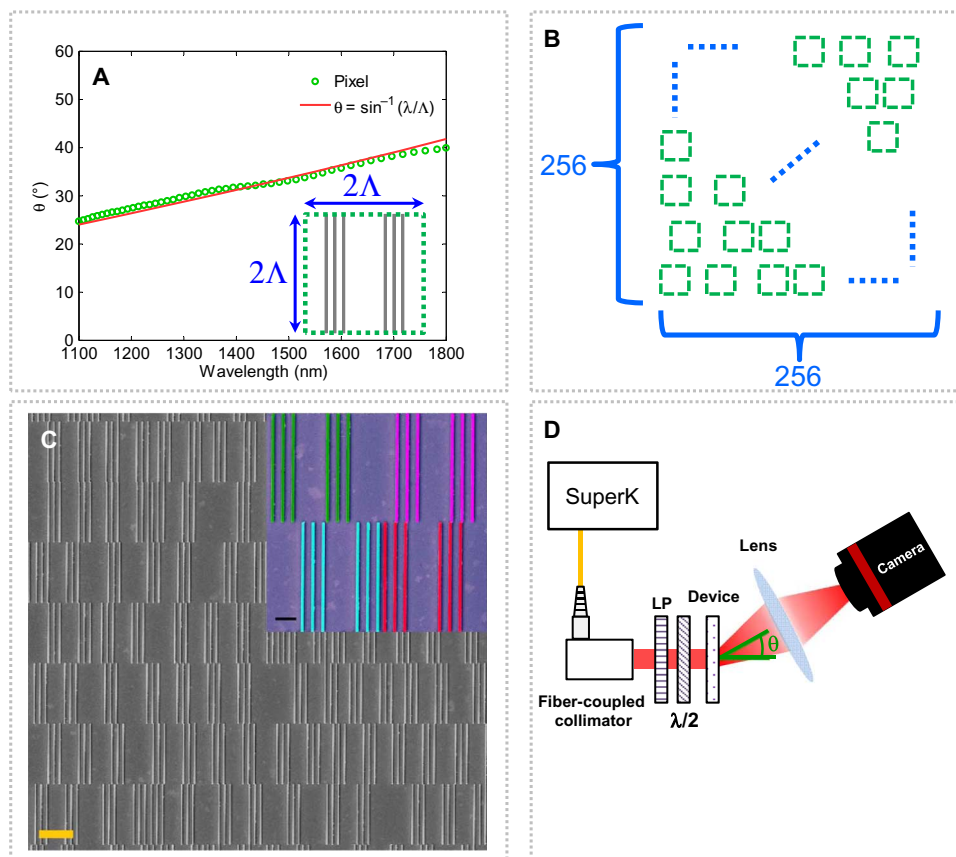

Fig. 1. Effective aperture made of subwavelength structured dielectric. (**A**) Schematic diagram of two apertures separated by a center-to-center distance D on a glass substrate. The phase shift associated with light propagating from the two apertures along the direction θ is denoted as $\Delta\varphi$. This phase difference is related to D and the wavelength, as shown in Eq. **1**. (**B**) Schematic diagram of a cross section of two generic pixels ($2\Lambda = 5.4\ \mu m$) of the hologram. Each pixel functions as an effective aperture consisting of six DRWs with subwavelength spacing ($S = 380\ nm$), width ($W = 120\ nm$), and height ($H = 400\ nm$). (**C**) Far-field [Real(E_y)^2] response of the effective aperture when the incident light is polarized along the y axis. This represents a two-dimensional finite-difference time domain simulation, where the DRWs are infinitely long along the y axis and the effective aperture extension along the x axis is $2\Lambda = 5.4\ \mu m$. Engineering the dispersive response of the DRWs results in highly directional diffraction, in which most of the transmitted light is funneled into the first orders whereas other diffraction orders are suppressed.

Fig. 2. Dispersion engineering and hologram design. (**A**) Diffraction angle of a pixel as a function of wavelength. Inset: Top view of the hologram pixel sized 5.4 μm × 5.4 μm (2Λ = 5.4 μm). The diffraction angle is calculated from the far-field response using finite-difference time domain simulations. The modeled diffraction angle closely follows the target angular dispersion $\theta = \sin^{-1}(\lambda/\Lambda)$ to cancel the wavelength dependence of the detour phase. (**B**) Schematic diagram showing the 256 × 256–pixel arrangement in the hologram. The required phase map is achieved through the displacement of each pixel. (**C**) Scanning electron microscopy (SEM) image of the device. Scale bar, 3 μm. Inset: A false-colored SEM image in which four pixels are highlighted with different colors. Scale bar, 1 μm. (**D**) Sketch of the experimental setup. The laser beam from a fiber-coupled supercontinuum laser is collimated by means of a fiber collimator. The polarization state of the laser beam is controlled by a linear polarizer (LP) followed by a half–wave plate ($\lambda/2$) before the laser beam illuminates the hologram (device). An image of the light distribution in the Fourier plane is obtained by means of a lens and an indium gallium arsenide (InGaAs) camera aligned along the direction of the first diffraction order. The lens is located at a focal length distance from both the device and the camera. For measurements in the visible range, the InGaAs camera is substituted by a color camera.

and has a high tolerance to the fabrication process, which is electron beam lithography in the present case. Our electron beam lithography (ELS-F125) has an ultrahigh beam positioning resolution (0.01 nm) that results in minimum phase mismatch (2) in the detour phase (fig. S3). Design tolerances are more demanding for those approaches where the phase modulation is achieved by changing the shape of subwavelength resonators or scatterers.

RESULTS AND DISCUSSION

As an example of our device functionality, a far-field intensity distribution corresponding to the 2015 IYL logo is designed (35). This device consists of 256 × 256 pixels, as shown in Fig. 2B. Figure 2C shows the SEM image of the fabricated device (see fig. S4 for the optical image of the device). A sketch of the experimental setup for image acquisition is shown in Fig. 2D. A thin lens is used to obtain an image in the Fourier

plane where the camera sensor is placed. Figure 3 (A to D) shows images of the intensity distribution generated by the hologram in the Fourier plane under NIR illumination. By design, the hologram provides the same image quality for all the wavelengths in the range λ = 1100 to 1800 nm, which is limited by our measurement setup (camera sensitivity and laser source range). This feature results from the dispersionless phase realization approach (Eq. 2). The dimension of the images in the reconstruction plane varies with wavelength according to the well-known relation $(N_i \lambda f)/L_i$, where f is the focal length of the lens and L_i and N_i are the device dimensions and number of pixels along the x and y axes, respectively (2).

The measured efficiency as a function of wavelength is reported in Fig. 3E. The efficiency is measured as the ratio of the optical power in the holographic image to the incident power. An efficiency as high as 75% is achieved. This value is close to the theoretical value (81%) of a binary phase grating optimized for a specific wavelength (3). Although our device is designed as a phase-only hologram, the use of
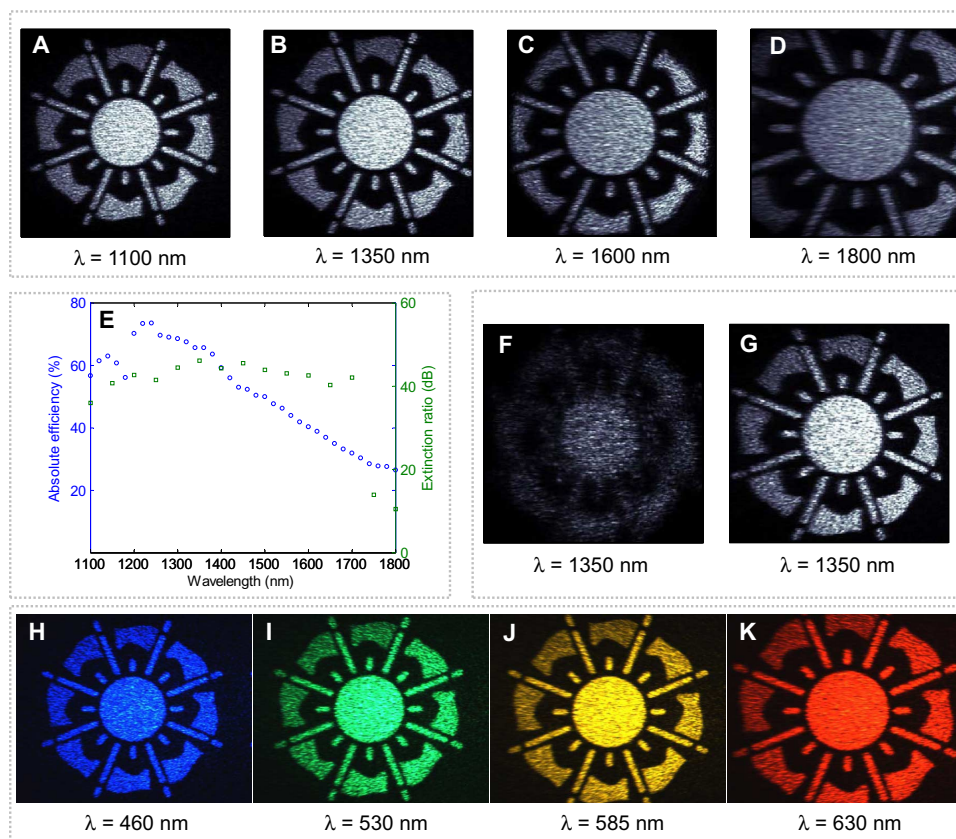
Fig. 3. Broadband phase distortion–free hologram. (**A** to **D**) Images generated when the hologram is illuminated with NIR light. (**E**) Absolute efficiency and extinction ratio (ER) as a function of wavelength. The drop in ER is due to the significant drop in the efficiency of the imaging camera at longer wavelengths. (**F** and **G**) Images corresponding to a hologram in which the IYL logo phase distribution is added to that of a Fresnel lens with a 2-cm total shift of the reconstruction plane. (F) Image captured under the same measurement conditions of (A) to (D). This image is blurry because the Fresnel lens phase profile encoded in the hologram moves the image plane 2 cm forward along the propagation direction. (G) The same image appears correctly in focus when the camera is moved 2 cm along the propagation direction. (**H** to **K**) Images generated by the hologram in the visible range. These images were captured by a color charge-coupled device camera.

subwavelength diffractive elements makes it possible to create images with high efficiency in the first orders only. The wavelength dependence of the efficiency can be interpreted in terms of the angular distribution of the diffracted power. In fact, from the simulation presented in Fig. 1C, it is evident that for wavelengths between 1150 and 1550 nm, most of the light goes only to the first orders, with a small (less than 10%) contribution to the zero order. However, as the wavelength is reduced, the angular response of the first orders narrows, resulting in a peak efficiency at around 1250 nm. Figure 3 (H to K) shows that the hologram (based on its dispersionless design) maintains its functionality even for visible light (see also figs. S5 and S6), although the transmittance of the device drops toward shorter wavelengths as a result of absorption from the silicon ridges.

The interaction of the DRWs with the incident light is highly polarization-dependent because of the DRWs' deep-subwavelength width and asymmetric cross section (the length is much larger than the width) (24). In other words, only light that is linearly polarized along the length of the DRWs (y axis) is efficiently diffracted, whereas light that is polarized along the width (x axis) is transmitted nearly nondiffracted (fig. S7). As a result of the polarization sensitivity of each pixel, our device is characterized by a high extinction ratio (ER) between orthogonal polarizations, within a broad

wavelength range (Fig. 3E). ER is defined as the ratio of normalized intensities in the images for two different polarizations [along the y and x axes for the IYL hologram and circularly left- and right-polarized for the chiral hologram (to be discussed later in the paper)].

This straightforward and reliable phase shift realization provides an opportunity for designing multifunctional devices. We further tested the capability of this concept by incorporating a Fresnel lens–like function to the phase map that corresponds to the 2015 IYL logo. This moves the reconstruction plane 2 cm forward in the light propagation direction. Figure 3 (F and G) shows the image at the previous focal position compared to the image in the new focal position. Image blurring and correct focusing are evident. It is worth noting that light focusing by the Fresnel hologram occurs along the diffraction direction ($\theta = 30°$ at $\lambda = 1350$ nm). Projection at large angles (for instance, $\theta \sim 42°$ at $\lambda = 1800$ nm) is a long-standing challenge (known as the shadow effect) that is overcome by our design. This opens the possibility of designing flat and compact optical components for imaging at a wide range of angles.

As further proof of the versatility of our approach, we designed a chiral hologram whose functionality depends on the handedness of the reference beam. For this task, the meta-element consists of nanofins similar to those in the studies of Khorasaninejad and Crozier (25) and
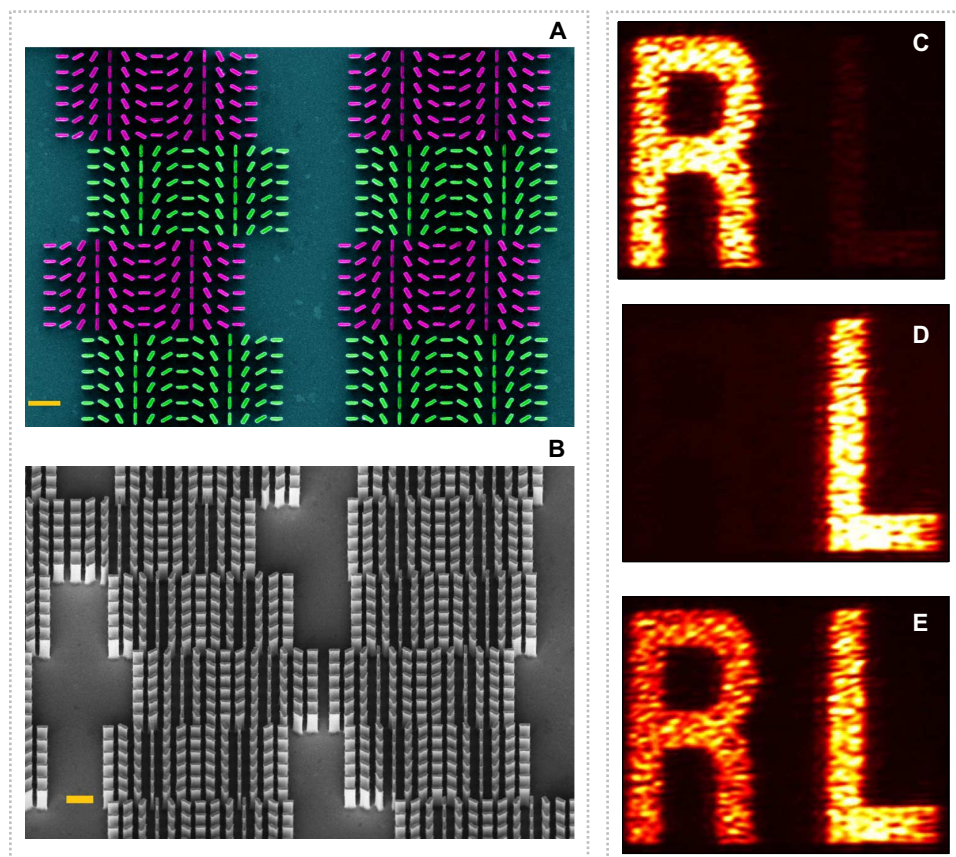
Fig. 4. Chiral hologram. (**A**) A false-colored SEM image of four pixels of the hologram. Each pixel consists of two parts: in purple, those that impart the required phase map for letter "L" and in green, those for the phase map for letter "R." Nanofins have a width (*W*) of 85 nm, a length (*L*) of 350 nm, a height (*H*) of 1000 nm, and a center-to-center distance of 500 nm. Scale bar, 1 μm. (**B**) Tilted view: SEM image of the hologram. Scale bar, 1 μm. (**C** to **E**) Images in the +1 diffraction order (false-colored) generated by the chiral hologram under different incident polarizations at λ = 1350 nm. Chiral hologram illuminated by (C) circularly right-polarized light, (D) circularly left-polarized light, and (E) linearly polarized light resulting in the appearance of the letters "R," "L," and "RL," respectively.

Lin *et al.* (*26*). When circularly polarized light passes through these structures, it is diffracted along a principal direction (θ) according to its handedness. Changing the light handedness results in the switching of the direction from θ to −θ analogously to other chiral subwavelength structured surfaces (*26, 29, 36*). According to what has been discussed so far, a phased array of such subwavelength structured pixels would result in the appearance of the designed intensity distribution along a specific direction only for circularly polarized light with the proper handedness. However, in the fabricated device, we divided each pixel into two parts (along the *y*-axis direction) and coupled half of it to one handedness and the other half to the opposite handedness (Fig. 4, A and B). The rotated nanofins in our design introduce a geometric phase similar to the rotated apertures of Shitrit *et al.* (*37*), known as the Berry-Pancharatman phase. In this way, the image displayed in the field of view of the optical system depends on the light handedness. Figure 4 (C to E) shows that a light intensity distribution corresponding to the letter "R" appears for right circular polarization, whereas it changes into the letter "L" for left circular polarization. In this case, a quarter–wave plate is used in the setup of Fig. 2D to generate circular polarization. For linear polarization, both letters appear. In addition, this device demonstrates

high values of absolute efficiency and ER, as well as a broadband functionality (figs. S8 and S9).

In conclusion, we used meta-elements to build phased pixels in flat and compact dielectric holograms with a broadband response. Depending on the subwavelength structured building blocks, different responses to light polarization states can be encoded for scalable polarimetric devices. Using dielectric materials instead of metals allows one to work in a transmission scheme with a transparent substrate while minimizing optical losses. Furthermore, lens-like optical elements working off-axis can be implemented for wearable devices, where lightness, compactness, and image quality are mandatory. In fact, although dynamic diffractive optical components, such as spatial light modulators, typically have a broadband response, they have a large footprint with respect to our devices. Here, we have shown that true optical functionality, such as imaging at an angle, can be achieved with a thin, small, lightweight, and efficient diffractive element fabricated on a transparent substrate that can be easily integrated in the design of near-to-eye displays and wearable optical systems. In addition, a new hologram with chiral imaging functionality has been demonstrated. Alternative fabrication methods, such as deep ultraviolet lithography and nanoimprinting, can facilitate

the mass production of our proposed devices. After the submission of this article, a related study (*38*) was reported.

METHODS

Evaluation of efficiency and ER
Efficiency was defined as the ratio of the total power of the first diffraction orders to the incident power. For the measurement of efficiency, power was measured by substituting the InGaAs camera (Fig. 2D) with a NIR photodetector (Thorlabs DET10D). The incident power was measured as light passing through an aperture (aluminum on a glass) that was of the same size as our holographic device. ER was defined as the ratio of normalized intensities in the images for two different polarizations (along the *y* and *x* axes for the IYL hologram and circularly left- and right-polarized for the chiral hologram).

SUPPLEMENTARY MATERIALS

Supplementary material for this article is available at http://advances.sciencemag.org/cgi/content/full/2/5/e1501258/DC1
Meta-element
Engineered dispersion of DRWs
Quality of the designed intensity distribution in the reconstruction plane
Optical image of the fabricated device
Illumination with visible light
Pixel far field in the visible range
Polarization-dependent response of the meta-element
Chiral hologram features
fig. S1. Meta-element.
fig. S2. Engineered dispersion of DRWs.
fig. S3. Hologram performance at different wavelengths.
fig. S4. Optical image of the holographic device.
fig. S5. Image of the 2015 IYL logo.
fig. S6. Far-field response of the meta-element in the visible range.
fig. S7. Polarization-selective meta-element.
fig. S8. Efficiency and ER of the chiral hologram.
fig. S9. Broadband chiral hologram.

REFERENCES AND NOTES

1. D. Gabor, A new microscopic principle. *Nature* **161**, 777–778 (1948).
2. J. W. Goodman, *Introduction to Fourier Optics* (Roberts & Company Publishers, Englewood, CO, ed. 3, 2005).
3. B. Kress, P. Meyrueis, *Applied Digital Optics* (Wiley, Hoboken, NJ, 2009).
4. B. Javidi, F. Okano, Eds., *Three-Dimensional Television, Video, and Display Technologies* (Springer, Berlin, 2002).
5. H. J. Coufal, G. T. Sincerbox, D. Psaltis, *Holographic Data Storage* (Springer-Verlag, Berlin, 2000).
6. T. C. Poon, in *Digital Holography and Three-Dimensional Display: Principles and Applications*, T. C. Poon, Ed. (Springer, New York, 2006), chap. 13, pp. 379–425.
7. O. Katz, E. Small, Y. Silberberg, Looking around corners and through thin turbid layers in real time with scattered incoherent light. *Nat. Photonics* **6**, 549–553 (2012).
8. D. Fattal, Z. Peng, T. Tran, S. Vo, M. Fiorentino, J. Brug, R. G. Beausoleil, A multi-directional backlight for a wide-angle, glasses-free three-dimensional display. *Nature* **495**, 348–351 (2013).
9. D. Fattal, J. Li, Z. Peng, M. Fiorentino, R. G. Beausoleil, Flat dielectric grating reflectors with focusing abilities. *Nat. Photonics* **4**, 466–470 (2010).
10. J. B. Pendry, A. Aubry, D. R. Smith, S. A. Maier, Transformation optics and subwavelength control of light. *Science* **337**, 549–552 (2012).
11. N. Yu, F. Capasso, Flat optics with designer metasurfaces. *Nat. Mater.* **13**, 139–150 (2014).
12. A. V. Kildishev, A. Boltasseva, V. M. Shalaev, Planar photonics with metasurfaces. *Science* **339**, 1232009 (2013).
13. N. Yu, P. Genevet, M. A. Kats, F. Aieta, J.-P. Tetienne, F. Capasso, Z. Gaburro, Light propagation with phase discontinuities: Generalized laws of reflection and refraction. *Science* **334**, 333–337 (2011).
14. A. Silva, F. Monticone, G. Castaldi, V. Galdi, A. Alù, N. Engheta, Performing mathematical operations with metamaterials. *Science* **343**, 160–163 (2014).
15. M. Ozaki, J. Kato, S. Kawata, Surface-plasmon holography with white-light illumination. *Science* **332**, 218–220 (2011).
16. S. Larouche, Y.-J. Tsai, T. Tyler, N. M. Jokerst, D. R. Smith, Infrared metamaterial phase holograms. *Nat. Mater.* **11**, 450–454 (2012).
17. N. I. Zheludev, Y. S. Kivshar, From metamaterials to metadevices. *Nat. Mater.* **11**, 917–924 (2012).
18. X. Ni, A. V. Kildishev, V. M. Shalaev, Metasurface holograms for visible light. *Nat. Commun.* **4**, 2807 (2013).
19. F. Monticone, N. M. Estakhri, A. Alù, Full control of nanoscale optical transmission with a composite metascreen. *Phys. Rev. Lett.* **110**, 203903 (2013).
20. W. T. Chen, K.-Y. Yang, C.-M. Wang, Y.-W. Huang, G. Sun, I.-D. Chiang, C. Y. Liao, W.-L. Hsu, H. T. Lin, S. Sun, L. Zhou, A. Q. Liu, D. P. Tsai, High-efficiency broadband meta-hologram with polarization-controlled dual images. *Nano Lett.* **14**, 225–230 (2014).
21. Y. Montelongo, J. O. Tenorio-Pearl, C. Williams, S. Zhang, W. I. Milne, T. D. Wilkinson, Plasmonic nanoparticle scattering for color holograms. *Proc. Natl. Acad. Sci. U.S.A.* **111**, 12679–12683 (2014).
22. W. Yu, T. Konishi, T. Hamamoto, H. Toyota, T. Yotsuya, Y. Ichioka, Polarization-multiplexed diffractive optical elements fabricated by subwavelength structures. *Appl. Opt.* **41**, 96–100 (2002).
23. J. Lin, P. Genevet, M. A. Kats, N. Antoniou, F. Capasso, Nanostructured holograms for broadband manipulation of vector beams. *Nano Lett.* **13**, 4269–4274 (2013).
24. M. Khorasaninejad, W. Zhu, K. B. Crozier, Efficient polarization beam splitter pixels based on a dielectric metasurface. *Optica* **2**, 376–382 (2015).
25. M. Khorasaninejad, K. B. Crozier, Silicon nanofin grating as a miniature chirality-distinguishing beam-splitter. *Nat. Commun.* **5**, 5386 (2014).
26. D. Lin, P. Fan, E. Hasman, M. L. Brongersma, Dielectric gradient metasurface optical elements. *Science* **345**, 298–302 (2014).
27. Y. Yifat, M. Eitan, Z. Iluz, Y. Hanein, A. Boag, J. Scheuer, Highly efficient and broadband wide-angle holography using patch-dipole nanoantenna reflectarrays. *Nano Lett.* **14**, 2485–2490 (2014).
28. P. Genevet, F. Capasso, Holographic optical metasurfaces: A review of current progress. *Rep. Prog. Phys.* **78**, 024401 (2015).
29. G. Zheng, H. Mühlenbernd, M. Kenney, G. Li, T. Zentgraf, S. Zhang, Metasurface holograms reaching 80% efficiency. *Nat. Nanotechnol.* **10**, 308–312 (2015).
30. M. Khorasaninejad, F. Aieta, P. Kanhaiya, M. A. Kats, P. Genevet, D. Rousso, F. Capasso, Achromatic metasurface lens at telecommunication wavelengths. *Nano Lett.* **15**, 5358–5362 (2015).
31. A. A. Michelson, On the spectra of imperfect gratings. *Astrophys. J.* **18**, 278–286 (1903).
32. B. R. Brown, A. W. Lohmann, Complex spatial filtering with binary masks. *Appl. Opt.* **5**, 967–969 (1966).
33. A. W. Lohmann, D. P. Paris, Binary Fraunhofer holograms, generated by computer. *Appl. Opt.* **6**, 1739–1748 (1967).
34. R. W. Gerchberg, W. O. Saxton, A practical algorithm for the determination of the phase from image and diffraction plane pictures. *Optik* **35**, 237–246 (1972).
35. International Year of Light and Light-Based Technologies, www.light2015.org/Home.html [accessed 10 August 2016].
36. U. Levy, H.-C. Kim, C.-H. Tsai, Y. Fainman, Near-infrared demonstration of computer-generated holograms implemented by using subwavelength gratings with space-variant orientation. *Opt. Lett.* **30**, 2089–2091 (2005).
37. N. Shitrit, S. Maayani, D. Veksler, V. Kleiner, E. Hasman, Rashba-type plasmonic metasurface. *Opt. Lett.* **38**, 4358–4361 (2013).
38. D. Wen, F. Yue, G. Li, G. Zheng, K. Chan, S. Chen, M. Chen, K. F. Li, P. W. Wong, K. W. Cheah, E. Y. Pun, S. Zhang, X. Chen, Helicity multiplexed broadband metasurface holograms. *Nat. Commun.* **6**, 8241 (2015).

Citation: M. Khorasaninejad, A. Ambrosio, P. Kanhaiya, F. Capasso, Broadband and chiral binary dielectric meta-holograms. *Sci. Adv.* **2**, e1501258 (2016).

Khorasaninejad *et al. Sci. Adv.* 2016;2:e1501258   13 May 2016

6 of 6

Science Advances

Broadband and chiral binary dielectric meta-holograms

The following resources related to this article are available online at
http://advances.sciencemag.org. (This information is current as of May 16, 2016):

Updated information and services, including high-resolution figures, can be found in the
online version of this article at:
http://advances.sciencemag.org/content/2/5/e1501258.full

Supporting Online Material can be found at:
http://advances.sciencemag.org/content/suppl/2016/05/10/2.5.e1501258.DC1

This article **cites 32 articles,** 7 of which you can be accessed free:
http://advances.sciencemag.org/content/2/5/e1501258#BIBL